ENVIRONMENTAL RESEARCH
LETTERS



LETTER • OPEN ACCESS

# Metrics for quantifying the efficiency of atmospheric $CO_2$ reduction by marine carbon dioxide removal (mCDR)

To cite this article: Kana Yamamoto *et al* 2024 *Environ. Res. Lett.* **19** 104053

ENVIRONMENTAL RESEARCH
LETTERS

OPEN ACCESS

RECEIVED
8 May 2024

REVISED
11 August 2024

ACCEPTED FOR PUBLICATION
28 August 2024

PUBLISHED
9 September 2024



LETTER

# Metrics for quantifying the efficiency of atmospheric $CO_2$ reduction by marine carbon dioxide removal (mCDR)

**Kana Yamamoto**[1,*], **Tim DeVries**[2,3] and **David A Siegel**[2,3]

[1] Interdepartmental Graduate Program in Marine Science, University of California Santa Barbara, Santa Barbara, CA 93106, United States of America
[2] Department of Geography, University of California Santa Barbara, Santa Barbara, CA 93106, United States of America
[3] Earth Research Institute, University of California Santa Barbara, Santa Barbara, CA 93106, United States of America
[*] Author to whom any correspondence should be addressed.

**E-mail:** kyamamoto@ucsb.edu

**Keywords:** carbon dioxide removal, ocean alkalinity enhancement, seawater carbon dioxide capture, carbon sequestration timescales

Supplementary material for this article is available online

## Abstract

Marine carbon dioxide removal (mCDR) is gaining interest as a tool to meet global climate goals. Because the response of the ocean–atmosphere system to mCDR takes years to centuries, modeling is required to assess the impact of mCDR on atmospheric $CO_2$ reduction. Here, we use a coupled ocean–atmosphere model to quantify the atmospheric $CO_2$ reduction in response to a CDR perturbation. We define two metrics to characterize the atmospheric $CO_2$ response to both instantaneous ocean alkalinity enhancement (OAE) and direct air capture (DAC): the cumulative additionality ($\alpha$) measures the reduction in atmospheric $CO_2$ relative to the magnitude of the CDR perturbation, while the relative efficiency ($\varepsilon$) quantifies the cumulative additionality of mCDR relative to that of DAC. For DAC, $\alpha$ is 100% immediately following CDR deployment, but declines to roughly 50% by 100 years post-deployment as the ocean degasses $CO_2$ in response to the removal of carbon from the atmosphere. For instantaneous OAE, $\alpha$ is zero initially and reaches a maximum of 40%–90% several years to decades later, depending on regional $CO_2$ equilibration rates and ocean circulation processes. The global mean $\varepsilon$ approaches 100% after 40 years, showing that instantaneous OAE is nearly as effective as DAC after several decades. However, there are significant geographic variations, with $\varepsilon$ approaching 100% most rapidly in the low latitudes while $\varepsilon$ stays well under 100% for decades to centuries near deep and intermediate water formation sites. These metrics provide a quantitative framework for evaluating sequestration timescales and carbon market valuation that can be applied to any mCDR strategy.

## 1. Introduction

Carbon dioxide removal (CDR) refers to the deliberate removal of $CO_2$ from the atmosphere and storage in a semi-permanent reservoir (NASEM 2019). If effective technologies for deploying CDR at large scales are developed, they could help reduce atmospheric $CO_2$ concentrations to keep warming to within 2 °C above pre-industrial values (IPCC 2022). The most direct CDR strategy is direct air capture (DAC), where $CO_2$ is stripped out of the atmosphere and stored in geologically permanent reservoirs (Keith *et al* 2006). Marine-based CDR (mCDR) strategies have also garnered interest due to the ocean's capacity to sequester carbon at the scale needed to offset anthropogenic $CO_2$ emissions (Fuss *et al* 2018, Friedlingstein *et al* 2023).

Marine CDR strategies lower atmospheric $CO_2$ ($C_{atm}$) by first reducing the dissolved $CO_2$ concentration in the ocean, which leads to increased oceanic uptake of $C_{atm}$ (NASEM 2022, Doney *et al* 2024). Most studies assessing mCDR efficacy have focused on the oceanic uptake of $C_{atm}$ assuming a constant atmospheric $CO_2$ concentration (Köhler *et al* 2013, He and Tyka 2023, Bach *et al* 2023a). This additional uptake of $C_{atm}$ relative to a counterfactual baseline without mCDR is referred to as the 'additionality' (Michaelowa *et al* 2019). However, assuming a constant $C_{atm}$ ignores the fact that perturbations in the ocean carbon reservoir ($C_{ocn}$) will inevitably lead to

perturbations in $C_{atm}$ and vice versa (Oschlies 2009, Keller *et al* 2018). For a more realistic estimate of mCDR additionality, the two-way exchange of carbon between the ocean and atmosphere must be considered.

Here, we use a coupled ocean–atmosphere model to quantify the magnitude and timescales of $C_{atm}$ reduction in response to small CDR perturbations. We focus our analysis on chemically mediated mCDR strategies, such as direct seawater capture and ocean alkalinity enhancement (OAE). Direct seawater capture refers to the electrochemical extraction of $CO_2$ from surface seawater and subsequent storage (Eisaman *et al* 2012), and OAE refers to the amendment of alkaline minerals and solutions to the surface ocean (Hartmann *et al* 2013, Bach *et al* 2019). Since OAE reduces dissolved $CO_2$ by shifting the $CO_2$ speciation in seawater, direct seawater capture and OAE are effectively equivalent if we assume that the alkalinity changes instantly. Therefore, we will refer to both direct seawater capture and OAE as 'instantaneous OAE'.

First, we introduce a model of the ocean–atmosphere carbon system linearized about the modern ocean state, which we use to simulate both DAC and instantaneous OAE (section 2). Then, we evaluate the additionality of both strategies and the relative efficiency of instantaneous OAE with respect to DAC to show that instantaneous OAE can be as effective as DAC in the long term, but with delays in efficacy and regional variability driven by differences in $CO_2$ equilibration and ocean circulation timescales (section 3). Finally, we address the model assumptions and simplifications, and discuss how the mCDR metrics introduced here inform the monitoring, reporting, verification, and market valuation of mCDR (section 4).

## 2. Methods

### 2.1. Ocean–atmosphere carbon model

A coupled ocean–atmosphere model is used to simulate the ocean and atmospheric carbon perturbation from CDR. For the ocean, we use a data-assimilated, global ocean circulation inverse model (OCIM). The OCIM estimates the climatological mean state of the ocean circulation for the modern ocean and casts it as a matrix transport operator (DeVries and Primeau 2011, DeVries 2014, 2022). Here we use the latest version, OCIM2-48L, which has a 2° horizontal resolution and 48 depth levels (Holzer *et al* 2021). The atmosphere is represented by a single well-mixed reservoir that exchanges $CO_2$ with each surface ocean grid cell. The distribution of dissolved inorganic carbon in the ocean (DIC, $\mu$mol kg$^{-1}$) and $CO_2$ in the atmosphere ($xCO_2$, ppm) is coupled by the air–sea $CO_2$ exchange:

$$\frac{\partial \mathrm{DIC}}{\partial t} = \mathbf{T}\cdot \mathrm{DIC} - \frac{1}{\rho z_1} F_{\mathrm{sea-air}} + J_{\mathrm{bio}} \quad (1)$$

$$\frac{\partial x\mathrm{CO}_2}{\partial t} = \frac{1}{M_{\mathrm{air}}} \int_A F_{\mathrm{sea-air}} \mathrm{d}A + J_{\mathrm{other}} \quad (2)$$

where $\mathbf{T}$ is the transport operator from OCIM2-48L (yr$^{-1}$), $F_{sea–air}$ is the sea-to-air $CO_2$ flux ($\mu$mol m$^{-2}$ yr$^{-1}$), $J_{bio}$ is the biological sources and sinks of DIC ($\mu$mol kg$^{-1}$ yr$^{-1}$), $J_{other}$ represents the combined fluxes from the terrestrial biosphere and anthropogenic $CO_2$ emissions (ppm yr$^{-1}$), $\rho$ is the seawater density (1025 kg m$^{-3}$), $z_1$ is the depth of the top OCIM2-48L layer (m), $M_{air}$ is the moles of air in the atmosphere ($1.7 \times 10^{20}$ mol), and d$A$ is the area of each model surface ocean grid cell (m$^2$). $F_{sea–air}$ is proportional to the gradient of the partial pressures of $CO_2$ in the ocean ($pCO_{2,ocn}$, $\mu$atm) and atmosphere ($pCO_{2,atm}$, $\mu$atm):

$$F_{\mathrm{sea-air}} = K_w K_0 \left(\mathrm{pCO}_{2,\mathrm{ocn}} - \mathrm{pCO}_{2,\mathrm{atm}}\right)\left(1 - f_{\mathrm{ice}}\right) \quad (3)$$

where $pCO_{2,atm}$ is directly proportional to $xCO_2$ assuming a constant sea surface pressure ($P_{atm}$) of 1 atm, $K_w$ is the piston velocity (m yr$^{-1}$) based on a quadratic relationship to 10 m wind speeds ($U_{10}$) (Wanninkhof 2014), $K_0$ is the $CO_2$ solubility in seawater (mol kg$^{-1}$ atm$^{-1}$), and $f_{ice}$ is the ice-covered fraction. $U_{10}$ and $f_{ice}$ are the annually averaged climatology from the NCEP/DOE Reanalysis II dataset (Kanamitsu *et al* 2002). $F_{sea–air}$ is positive when there is a net flux of $CO_2$ into the atmosphere.

$F_{sea–air}$ is non-linear with respect to DIC but can be approximated by linearizing the carbonate system about the modern ocean state such that the air–sea $CO_2$ equilibration timescale ($\tau_{CO2}$) is:

$$\tau_{\mathrm{CO}_2} = \frac{z_1 \beta}{K_w R} \quad (4)$$

where $\beta$ is the equilibrium ratio of DIC to dissolved $CO_2$ in seawater and $R$ is the Revelle factor (Broecker and Peng 1974, Nowicki *et al* 2024). The global distribution of $\tau_{CO2}$ is plotted in figure S1. The ocean carbonate parameters ($\beta$, $R$, $K_0$) are solved using CO2SYS (van Heuven *et al* 2011) with inputs of DIC and total alkalinity from the GLODAPv2 mapped climatology (Lauvset *et al* 2016) and phosphate, silicate, sea surface temperature, and sea surface salinity taken from the annual climatologies of World Ocean Atlas 2018 (Boyer *et al* 2018).

### 2.2. Modeling the impacts of CDR

We simulate two CDR strategies: DAC and instantaneous OAE. The modeled carbon perturbation due to CDR is the difference between the simulation with and without CDR, noted as. By linearizing $F_{sea–air}$

with respect to DIC using $\tau_{CO2}$, we can directly model this perturbation ($\Delta$) in the ocean and atmosphere (see supplementary text for derivation):

$$\frac{\partial \Delta \mathrm{DIC}}{\partial t} = \mathbf{T} \cdot \Delta \mathrm{DIC} - \frac{1-f_{\mathrm{ice}}}{\rho \tau_{\mathrm{CO2}}} \left( \Delta \mathrm{DIC} - \frac{K_o \beta}{R} \mathrm{P_{atm}} \Delta \mathrm{xCO_2} \right) - \Delta J_{\mathrm{CDR,ocn}}(t,r) \quad (5)$$

$$\frac{\partial \Delta \mathrm{xCO_2}}{\partial t} = \frac{z_1}{M_{\mathrm{air}}} \int_A \frac{1-f_{\mathrm{ice}}}{\tau_{\mathrm{CO2}}} \left( \Delta \mathrm{DIC} - \frac{K_o \beta}{R} P_{\mathrm{atm}} \Delta \mathrm{xCO_2} \right) \mathrm{d}A - \Delta J_{\mathrm{CDR,atm}}(t) \quad (6)$$

where $\Delta J_{\mathrm{CDR,ocn}}(t,r)$ and $\Delta J_{\mathrm{CDR,atm}}(t)$ are the finite CDR perturbation applied in the ocean or atmosphere, respectively, and '$r$' indicates location of the CDR deployment and '$t$' is the time since its onset. We assume that the biological pump ($J_{\mathrm{bio}}$) and the terrestrial flux and anthropogenic emissions ($J_{\mathrm{other}}$) do not respond to the perturbation. Thus, $J_{\mathrm{bio}}$ and $J_{\mathrm{other}}$ are identically zero. For DAC, we introduced a $\Delta J_{\mathrm{CDR,atm}}$ of 1 ppm yr$^{-1}$ for the first 30 days of the simulation. Though we attribute $J_{\mathrm{CDR,atm}}$ to the capture of $C_{atm}$, this effect can also be achieved via negative or avoided emissions. For instantaneous OAE, we introduced a $\Delta J_{\mathrm{CDR,ocn}}$ of 1 $\mu$mol kg$^{-1}$ yr$^{-1}$ in the top ocean layer for the first 30 days. We applied this perturbation to a single surface ocean grid at a time and repeated the simulation for all surface ocean grids individually. The 30 day duration is an approximation for a finite, one-time application of CDR (e.g. ship-based OAE). Note that continuous, long-term deployments may lead to significant changes in the near-field or global ocean carbonate system, which would fall outside the scope of our linearized model. For all simulations, $\Delta J_{\mathrm{CDR,atm}}$ and $J_{\mathrm{CDR,ocn}}$ were set to 0 after 30 days and the models were run for 1000 years. We used a daily time-step for the first 90 days, a monthly time-step thereafter until Year 5, an annual time-step thereafter until Year 100, a 10 year time-step thereafter until Year 500, and a 100 year time-step thereafter until Year 1000. For instantaneous OAE, simulations for only 100 randomly selected grids were completed for the full 1000 years. The rest were simulated for only 100 years. This reduced the computation time while still providing a robust estimate of spatial variability.

At each time-step, we calculated the net change in atmospheric carbon ($\Delta C_{atm}$), which is the product of $M_{\mathrm{air}}$ and $\Delta xCO_2$, and the total amount of carbon removed from the ocean–atmosphere system via CDR ($\Delta C_{CDR}$). For DAC, $\Delta C_{CDR}$ is the product of $M_{\mathrm{air}}$ and the time-integrated $\Delta J_{\mathrm{CDR,atm}}(t)$. For instantaneous OAE, $\Delta C_{CDR}$ is the product of seawater density and the time- and volume-integrated $\Delta J_{\mathrm{CDR,ocn}}(t,r)$. $C_{CDR}$ is constant after 30 days, since no further CDR perturbation is applied. The ratio between $C_{atm}$ and $C_{CDR}$ is the 'cumulative additionality' ($\alpha$):

$$\alpha(t,r) = \frac{\Delta C_{\mathrm{atm}}(t,r)}{\Delta C_{\mathrm{CDR}}(t,r)} \times 100\%. \quad (7)$$

Normalizing the cumulative additionality of mCDR ($\alpha_{\mathrm{mCDR}}(t,r)$) to that of DAC ($\alpha_{\mathrm{DAC}}(t)$) provides a metric that compares the efficacy of mCDR to that of DAC, which we call the 'relative efficiency' ($\varepsilon$):

$$\varepsilon(t,r) = \frac{\alpha_{m\mathrm{CDR}}(t,r)}{\alpha_{\mathrm{DAC}}(t)} \times 100\%. \quad (8)$$

Since we applied the perturbation for instantaneous OAE to each surface ocean grid individually, we quantified $\alpha$ and $\varepsilon$ for each surface grid, $r$, as a function of time, t.

The present modeling approach can be applied to assess the efficacy of other mCDR strategies, such as iron fertilization and macroalgal sequestration, by changing the parameterization of $J_{\mathrm{CDR,ocn}}$ to properly reflect the impacts of these methods. The focus here is on assessing the carbon sequestration timescales via instantaneous OAE to demonstrate the roles of gas exchange and ocean mixing and circulation processes on mCDR metrics.

## 3. Results

The global mean cumulative additionalities ($\alpha$) for DAC and instantaneous OAE differ in the first several decades after CDR deployment but converge after ~40 years (figure 1(a)). For DAC, $\alpha$ is initially 100%, but gradually declines to 47% after 100 years post-deployment and to 21% after 1000 years. In contrast, the global mean $\alpha$ for instantaneous OAE is initially zero, increases to a maximum of 65% after 9 years, declines to 46% after 100 years, and is nearly equivalent to DAC thereafter. The spread in the instantaneous OAE $\alpha$ values are due to differences in deployment site characteristics, which we discuss later. It is important to note that this spread does not encompass the full range of uncertainties in the response of the ocean–atmosphere system to instantaneous OAE and DAC, due to simplifications and assumptions of our model as discussed in section 4.

To understand the difference between the DAC and instantaneous OAE $\alpha$ values in the first 100 years, we break them down into different phases. For DAC, there are only two phases: the initialization and outgassing phase. In the initialization phase for DAC, $CO_2$ is removed directly from the atmosphere (i.e. $\Delta C_{atm} = \Delta C_{CDR}$), resulting in an $\alpha$ of 100%. Then in the outgassing phase, the global reduction in $pCO_{2,atm}$ as a result of DAC leads to ocean outgassing, which offsets the initial $C_{atm}$ reduction, leading to a decline in $\alpha$. For instantaneous OAE, there are

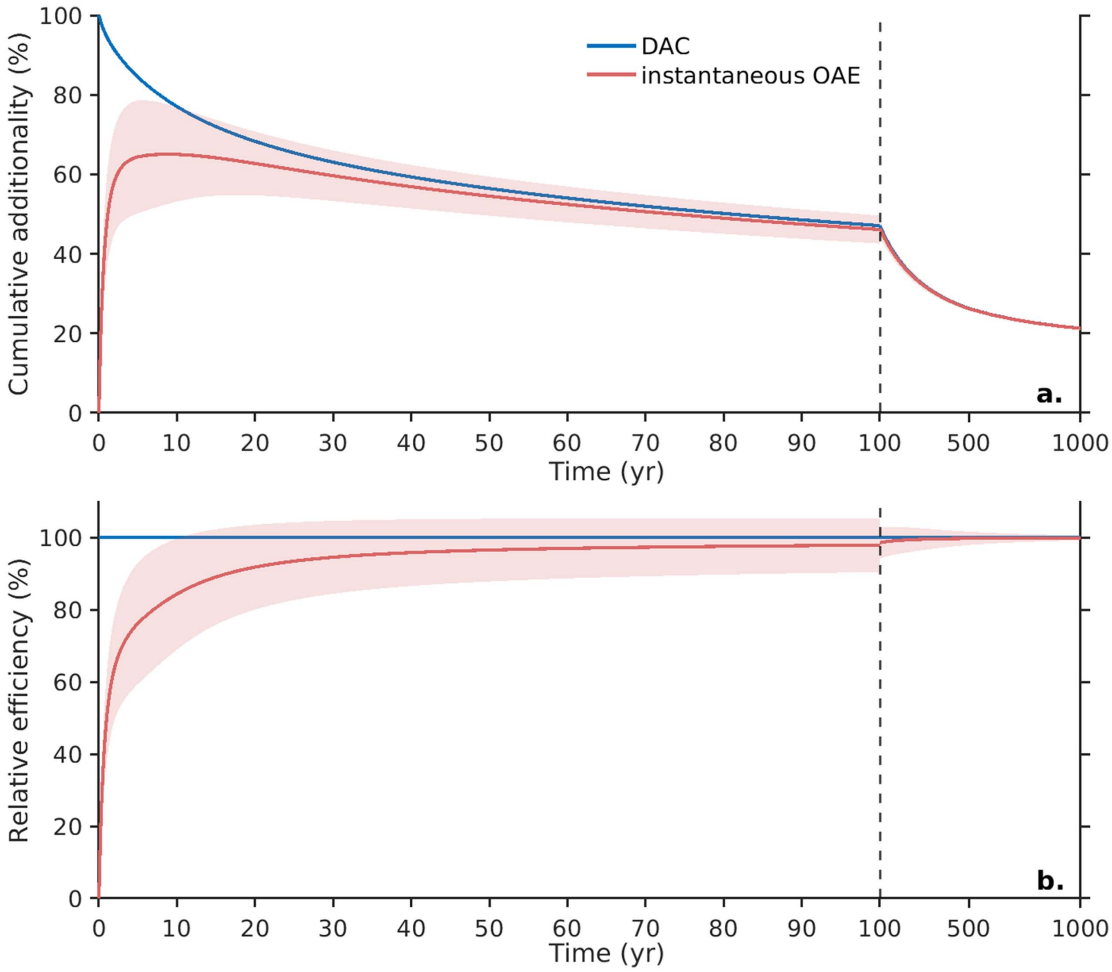


**Figure 1.** (a) Global cumulative additionality curves and (b) global relative efficiency curves for finite carbon removal via DAC and instantaneous OAE. For the first 100 years in both panels, the solid line and shading for instantaneous OAE indicate the global mean and spatial standard deviation, respectively, of each metric across all surface grids with an annual mean ice-cover ⩽50%. After 100 years, the solid line and shading for instantaneous OAE indicate the mean and spatial standard deviation, respectively, across 100 randomly selected surface grids with an annual mean ice-cover ⩽50%. The blue and red lines overlap after 100 years.

three phases: the initialization, ingassing, and outgassing phase. The initialization phase for instantaneous OAE removes $CO_2$ from the surface ocean but not yet from the atmosphere (i.e. $\Delta C_{atm} = 0$), resulting in an $\alpha$ of zero. In the ingassing phase, the $CO_2$-deficient surface water begins to equilibrate with the atmosphere and draws down $C_{atm}$, leading to an increase in $\alpha$. After the $CO_2$-deficient water mass is fully equilibrated with the atmosphere, or is subducted into the interior ocean where it no longer interacts with the atmosphere, we transition into the outgassing phase as in DAC. Values of $\alpha$ for DAC and instantaneous OAE converge because in each case the ocean–atmosphere system equilibrates to the same, new steady-state where the carbon deficit is redistributed across these reservoirs.

Clearly, no CDR strategy can sustain 100% cumulative additionality due to the re-partitioning of $CO_2$ between the ocean and atmosphere. This is important to recognize when evaluating the actualized $C_{atm}$ reduction, but this decline in efficacy will be true for any emissions intervention. Therefore, it is helpful for valuation purposes to define the relative efficiency ($\varepsilon$) (figure 1(b)). The global mean $\varepsilon$ for instantaneous OAE reaches 90% after 17 years, which represents the time-lag associated with the equilibration of negative DIC anomalies due to both mixing and gas exchange. After 100 years, $\varepsilon$ reaches 98%. This indicates that on a global average, instantaneous OAE is nearly as effective as DAC after a few decades.

Regional differences in the efficacy of instantaneous OAE are expected due to geographic variations in $CO_2$ equilibration and ocean ventilation timescales. The $\alpha$ and $\varepsilon$ curves for instantaneous OAE at eight different locations are shown in figure 2. From these curves, we can compare the magnitude and timescale of mCDR efficacy through the maximum cumulative additionality ($\alpha_{max}$) and the time for $\varepsilon$ to reach 90% ($\tau_{90\%}$), respectively. Between the subpolar regions, Station Papa in the North Pacific reaches an $\alpha_{max}$ of 79% in 4.25 years, but at the Porcupine Abyssal Plain (PAP), $\alpha_{max}$ is only 44% and takes 15 years to reach (figure 2(a)). This leads to a higher $\varepsilon$ for Station Papa in the first 100 years with

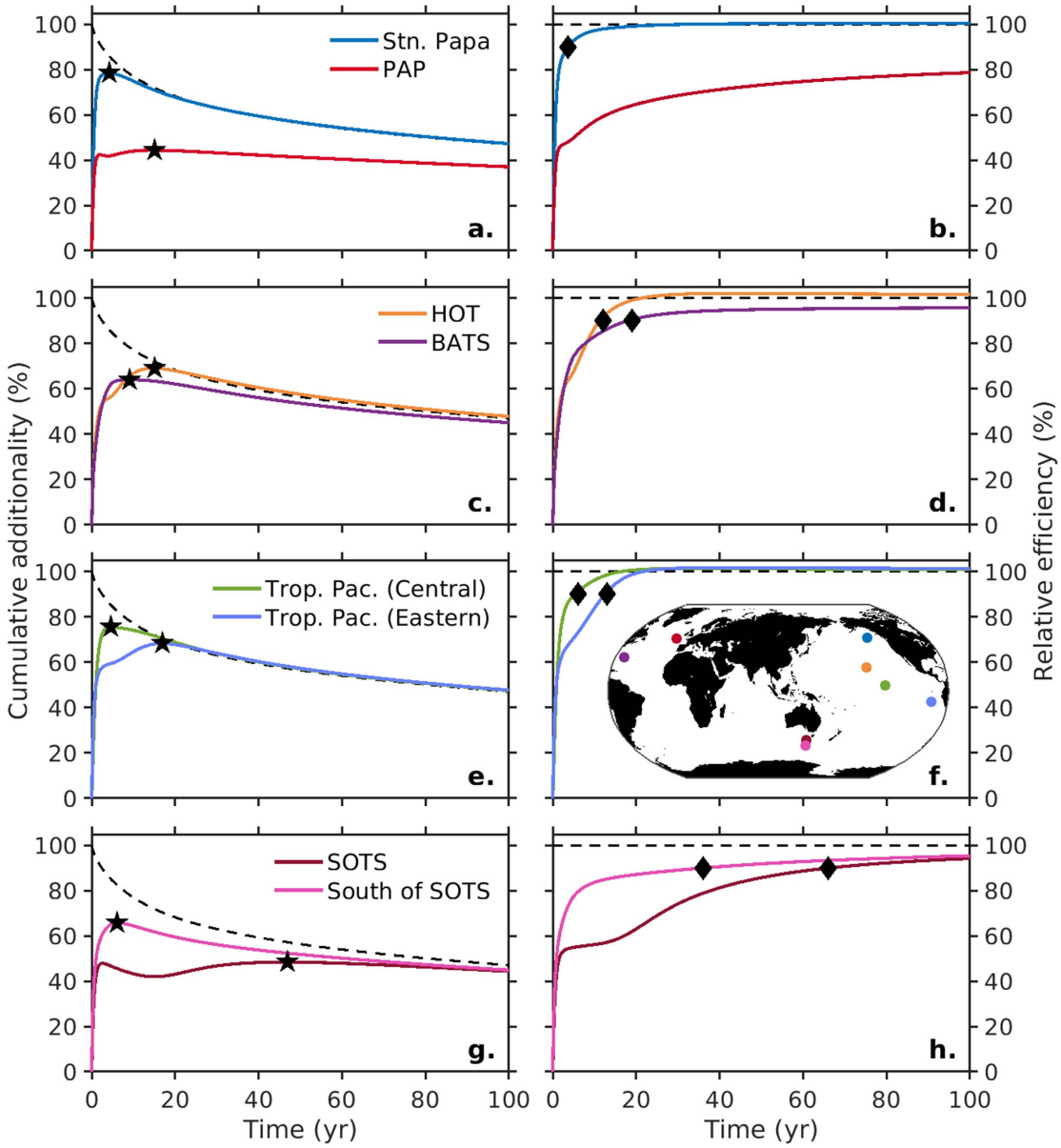


**Figure 2.** (a), (c), (e), (g) Cumulative additionality and (b), (d), (f), (h) relative efficiency curves for instantaneous OAE at 8 different sites: (a), (b) Station Papa (50° N, 145° W) in the North Pacific and Porcupine Abyssal Plain (PAP; 48° N, 16° W) in the North Atlantic; (c), (d) Hawaii Ocean Time-series site (HOT; 22° N, 158° W) in the Northern Pacific subtropics and Bermuda Atlantic Time-series site (BATS; 31° N, 64° W) in the Northern Atlantic subtropics; (e), (f) Tropical Pacific sites in Central (5° N, 140° W) and Eastern Pacific (10° S, 90° W); and (g), (h) Southern Ocean Time-series site (SOTS; 46° S, 140° E) and a site 4° south of SOTS (50° S, 140° E). The dashed black lines are for DAC. Stars mark the maximum cumulative additionality ($\alpha_{max}$) and diamonds mark the time to 90% relative efficiency ($\tau_{90\%}$) for each site.

a $\tau_{90\%}$ of 3.75 years while at PAP, $\varepsilon$ is only 78% after 100 years (figure 2(b)). Both sites have similar $\tau_{CO2}$ of roughly 30 days (figure S1). However, in the North Atlantic, surface waters are subducted more rapidly than the timescale of $CO_2$ equilibration due to deep water formation, resulting in less $C_{atm}$ drawdown. In the subpolar North Pacific, a longer surface residence time allows for a more complete equilibration. Variations in $\tau_{CO2}$ also impact mCDR efficacy by altering the rate of $C_{atm}$ drawdown. The two subtropical sites in the Pacific and Atlantic have a more gradual ingassing phase than the subpolar sites owing to longer $\tau_{CO2}$ (figure 2(c)). At the Hawaii Ocean Time-series (HOT), $\alpha_{max}$ of 69% is reached after 15 years. At the Bermuda Atlantic Time-series (BATS), $\alpha_{max}$ is 64% after 9 years. Longer $\tau_{CO2}$ and lower $\alpha_{max}$ values contribute to longer $\tau_{90\%}$ at HOT (12 years) and BATS (19 years) relative to Station Papa (figure 2(d)). Slight variations between HOT and BATS are likely due to regional differences in subduction and ventilation patterns.

Circulation patterns can cause differences in mCDR efficacy even for sites in close proximity. For example, a site in the Central Tropical Pacific has a relatively high $\alpha_{max}$ (75% in 4.5 years), but a site within the upwelling region of the Eastern Tropical Pacific has a weaker and more prolonged response ($\alpha_{max}$ = 68% in 17 years) (figure 2(e)). This leads to

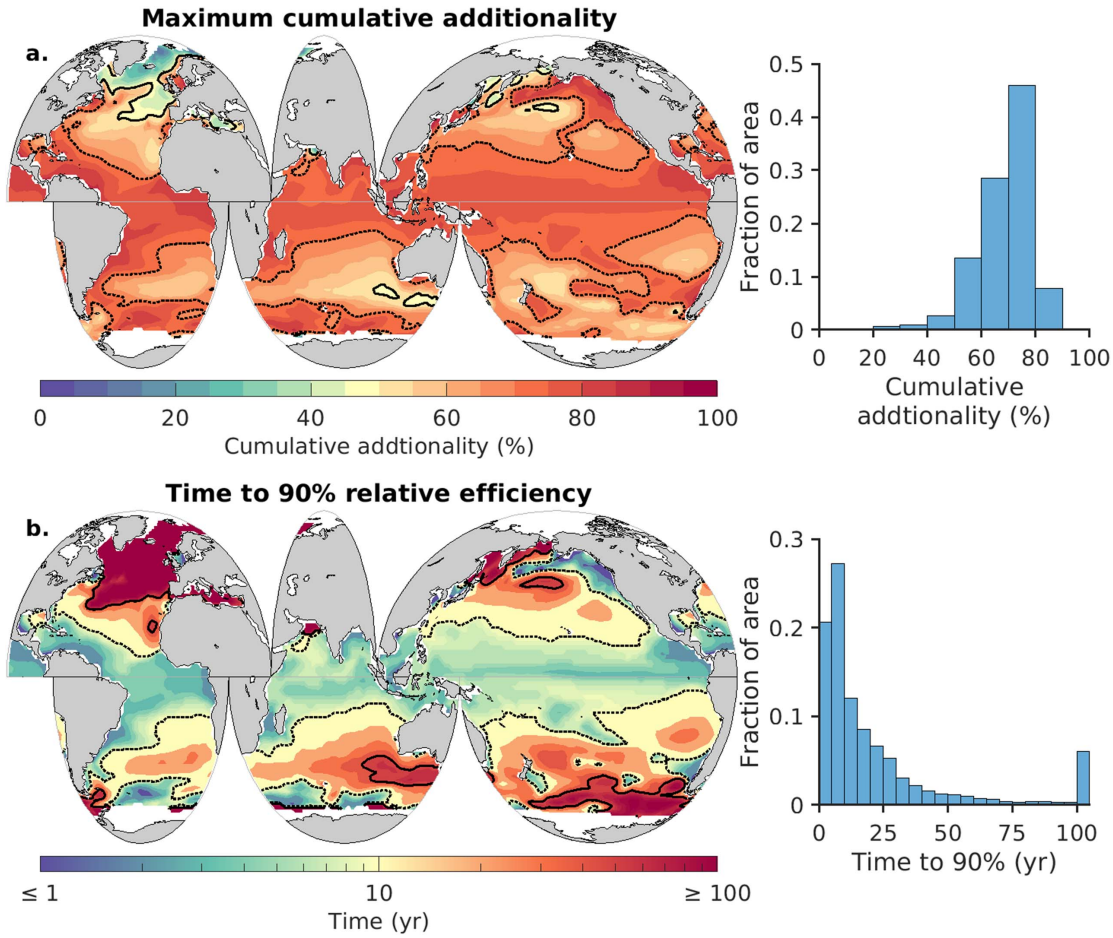


**Figure 3.** (a) Maximum cumulative additionality ($\alpha_{max}$) for the deployment of instantaneous OAE at each surface grid. Dashed and solid black contour marks an $\alpha_{max}$ of 70% and 50%, respectively. Histogram to the right shows the area-weighted global distribution of $\alpha_{max}$. (b) Time to reach 90% relative efficiency ($\tau_{90\%}$) at each surface grid. Dashed and solid black contours mark 10 and 50 years, respectively. Histogram shows the area-weighted global distribution of $\tau_{90\%}$. The rightmost bar in the histogram shows all the $\tau_{90\%}$ values greater than 100 years. Surface grids with an annual mean ice-cover >50% were omitted for all analyses. Time snapshot maps of cumulative additionality and relative efficiency are shown in supplemental figures S2 and S3, respectively.

a difference in $\tau_{90\%}$ by a factor of two between these sites with a value of 6 years versus 13 years at the Central and Eastern sites, respectively (figure 2(f)). However, $\alpha$ converges in these two locations after 20 years, so the efficacy at these sites is effectively the same after a couple decades. Local heterogeneity is even more pronounced in the Southern Ocean (figures 2(g) and (h)). At the Southern Ocean Time-series (SOTS), $\alpha$ remains relatively low, reaching a maximum of 48% after 47 years (figure 2(g)). In contrast, just 4° south of SOTS, $\alpha_{max}$ is 66% and realized in only 6 years. This difference is caused by the oceanographic boundary marked by the polar front (Bach *et al* 2023b). At both sites, $\alpha$ increases at a similar rate after the initialization phase because $\tau_{CO2}$ is similar (figure S1). However, at SOTS, which lies north of the polar front, surface waters are subducted to form mode waters which halts the equilibration of the negative $CO_2$ anomaly, similar to sites near deep water formation like PAP (figure 2(a)). But unlike deep waters, these mode waters resurface more quickly, allowing for further $C_{atm}$ uptake and leading to a distinct secondary ingassing phase (figure 2(g)). This allows for a boost in the $\varepsilon$ curve near Year 20 and leads to a shorter $\tau_{90\%}$ of 67 years at SOTS (figure 2(h)) compared to >100 years at PAP (figure 2(b)). Still, the site south of SOTS has a $\tau_{90\%}$ of 36 years (figure 2(h)), showcasing the impact of circulation. Thus, oceanographic boundaries such as large-scale fronts can cause large geographic variability in $C_{atm}$ uptake.

A global map of $\alpha_{max}$ further illustrates the influence of air–sea equilibration timescales and subduction patterns on the efficacy of instantaneous OAE (figure 3). Values of $\alpha_{max}$ are consistently high in the tropics (figure 3(a)) because surface waters there remain at the surface long enough to reach near-complete air–sea $CO_2$ equilibration. High $\alpha_{max}$ values also occur in the eastern North Pacific and south of 50°S in the Atlantic and Indian sectors of the Southern Ocean (figure 3(a)). Regions near mode-water formation have lower values of $\alpha_{max}$, and $\alpha_{max}$ is lowest in the subpolar North Atlantic near locations of deep-water formation (figure 3(a)). These results are consistent with studies that showed high

DIC equilibration efficiency off the coast of Brazil and in the eastern Bering Sea, and low equilibration efficiency near Iceland (Wang *et al* 2023, Bach *et al* 2023a). The global median $\alpha_{max}$ is 71% with a 10th and 90th percentile range of 56–79%. No model grid reached an $\alpha_{max}$ value of 100%. This is because the ingassing of additional $C_{atm}$ and the outgassing of $C_{ocn}$ occurs in tandem. Thus, even if a $CO_2$-deficient water mass achieves complete air–sea equilibration, the simultaneous outgassing of $CO_2$ during this time reduces the net $C_{atm}$ drawdown.

Global values of $\tau_{90\%}$ are generally inversely related to $\alpha_{max}$. Regions where $\alpha_{max}$ is greater than the median tend to have $\tau_{90\%}$ values of less than 10 years (figure 3(b)). Conversely, regions where $\alpha_{max}$ is 50% or lower generally exhibit $\tau_{90\%}$ values of 50 or more years (figure 3(b)). The global median $\tau_{90\%}$ is 11 years with a 10th and 90th percentile range of 3.8–58 years. In 6% of the ocean surface with an annual mean ice-cover $\leqslant$50%, $\tau_{90\%}$ is over 100 years.

## 4. Discussion

### 4.1. Model assumptions and simplifications

We made several assumptions to estimate OAE and DAC efficacy in this study. First, potential changes in physical forcings associated with climate change such as changes in ocean circulation, winds, and temperature were ignored. Second, we assumed that the biological pump is not affected by OAE or DAC. Third, we linearized the model assuming a constant carbonate chemistry with a constant Revelle factor, though the Revelle factor will increase as the ocean takes up more anthropogenic carbon (Bates *et al* 2014, Fassbender *et al* 2018). Understanding how future changes in the Earth system will affect the durability of any mCDR action is important, but future pathways of emissions and climate are highly uncertain.

In a case study to examine the impact of centennial changes in the Revelle factor, we estimated the cumulative additionality ($\alpha$) for DAC with the full non-linear $CO_2$ system chemistry using a medium and high emissions scenario (Clarke *et al* 2007, Riahi *et al* 2007). For the medium emissions scenario, atmospheric $CO_2$ was ~450 ppm and $\alpha$ was 15% higher than the linearized estimate after 100 years (figure S4). For the high emissions scenario, atmospheric $CO_2$ was ~900 ppm and $\alpha$ was 31% higher than the linearized estimate after 100 years (figure S4). Increased emissions lead to higher Revelle factors, resulting in proportionally larger changes in $pCO_{2,ocn}$ with changes in ocean DIC. Though considering changes in the ocean carbonate system is certainly important for estimating $\alpha$, other factors such as temperature and ocean circulation changes (Riebesell *et al* 2009, Goris *et al* 2018) are likely to contribute similar or greater uncertainty to our model estimates at century timescales.

Our model also lacks seasonality, which may be important to consider during the deployment phase. The initial $C_{atm}$ uptake is governed by $CO_2$ equilibration timescales and ocean circulation (figure 2), which vary seasonally. Jones *et al* (2014) showed strong seasonality in $CO_2$ equilibration timescales in the high latitudes with shallower mixed layers driving a shortening of the equilibration timescale in hemispheric summers. Shorter equilibration timescales with weaker deep-water formation in the summers could potentially boost initial $\alpha$ values for summertime mCDR deployment in locations like the North Atlantic and the Southern Ocean. Conversely, longer equilibration timescales due to deeper mixed layers coupled with stronger deep-water formation could decrease mCDR efficacy in these locations during hemispheric winters. This may be particularly important for biotic mCDR strategies, such as iron fertilization and macroalgal biomass sequestration. Future studies should aim to assess the importance of seasonality on mCDR efficacy.

We also simplified the model representation of the atmosphere and terrestrial biosphere. Our use of a uniform atmosphere creates instances where relative efficiency exceeds 100% in some grids, which seems unlikely in the real ocean (figure 1(b)). But based on similar timescales of inter-hemispheric exchange within the troposphere and the air–sea $CO_2$ equilibration (both on the order of 1 year) and the much longer timescale of global ocean mixing (on the order of 1000 years), this is a reasonable simplification for understanding the carbon perturbations across the ocean and atmosphere on annual to centennial timescales. Our model also lacks an interactive terrestrial biosphere whose impact to Earth's carbon system is controlled by its physiological response to changes in $C_{atm}$ and temperature (Arora *et al* 2020). For a full assessment of the carbon sequestration efficiency for any CDR strategy, the inclusion of an interactive terrestrial biosphere is crucial (Keller *et al* 2018).

Lastly, our model estimates are for an idealized case of instantaneous OAE, and we did not consider the technical inefficiencies or delays related to OAE deployment. This includes the carbon emissions associated with mineral mining (Foteinis *et al* 2023), loss of mineral amendments through particle sinking (Yang and Timmermans 2024), offsets to the increase in alkalinity due to modifications in natural alkalinity (Bach 2024), and delays between mineral applications and $CO_2$ reduction due to slow mineral dissolution (Fakhraee *et al* 2023). Therefore, the results presented here can be thought of as one component within a holistic life cycle evaluation when determining the costs and benefits associated with mCDR.

### 4.2. Considerations for mCDR monitoring, reporting, verification, and valuation

Our estimates of mCDR efficacy highlight the challenges associated with monitoring, reporting, and

verification (MRV) of mCDR. For instantaneous OAE, peak $C_{atm}$ reduction will take at least one year even in highly efficient regions and around 9 years on average (figure 1(a)). During this time, the perturbations introduced by mCDR will have spread across much of the global ocean (He and Tyka 2023), and tracking these imperceptible changes across space and time will be nearly impossible (Ho *et al* 2023). The simultaneous carbon cycle response during this ingassing phase will also need to be evaluated to quantify the net $C_{atm}$ reduction. When measuring the $C_{atm}$ response to CDR, it is important for MRV practitioners to be aware that neither DAC nor instantaneous OAE will lead to 100% cumulative additionality. At best, only around 50% of the initial CDR effort for DAC or instantaneous OAE is reflected in $C_{atm}$ after a century (figure 1(a)). This fraction could be near zero for biotic mCDR strategies that do not involve permanent reductions in the carbon inventory, unless a large fraction of exported carbon reaches below 1000 m or is buried as sediment (Siegel *et al* 2021).

This paper also serves to clarify the usage of 'additionality'. Many previous studies have estimated additionality using a fixed $C_{atm}$ (Köhler *et al* 2013, He and Tyka 2023, Bach *et al* 2023a). But cumulative additionality ($\alpha$) cannot be quantified with a fixed $C_{atm}$ because it depends on the drawdown of atmospheric $CO_2$ (equation (7)). However, we find that the additionality estimates using a fixed $C_{atm}$ ($A_{fixed}$) is a good approximation for relative efficiency ($\varepsilon$). We modeled $A_{fixed}$, defined as the ratio of oceanic carbon uptake under a fixed $C_{atm}$ relative to $C_{CDR}$ (Bach *et al* 2023a), for eight sites (figure S5). Across these sites, $A_{fixed}$ and $\varepsilon$ are similar; at Year 100, $\varepsilon$ is 0.7–6.0% higher than $A_{fixed}$.

While $\alpha$ is an important metric for tracking $C_{atm}$ reduction, $\varepsilon$ may be more appropriate for valuation of mCDR strategies. Since DAC is equivalent to negative emissions, the valuation for DAC can be scaled for mCDR using $\varepsilon$. For instantaneous OAE, $\varepsilon$ eventually approaches 100% everywhere, but the timescale of this approach to unity varies depending on deployment location (figure 2). Any carbon valuation scheme should take into account the full temporal evolution of $\varepsilon$ for a given deployment location, since the price of carbon emissions varies with time and may be discounted for future emissions relative to present ones (Herzog *et al* 2003).

## 5. Conclusion

We provide two metrics of mCDR efficacy, cumulative additionality and relative efficiency, that account for the magnitude and timescales of carbon exchange between the ocean and atmosphere. We focused our analysis on instantaneous OAE and found that OAE is most suitable in the tropics and the northeastern Pacific and largely unsuitable in subpolar regions. Although our findings are subject to numerous approximations, the numerical framework and metrics developed here are flexible and broadly applicable to evaluating other mCDR strategies. As such, we urge future framers of CDR carbon markets to consider the use of these metrics when carbon markets are established.

## Data availability statement

The data that support the findings of this study are openly available at the following URL/DOI: (https://doi.org/10.5281/zenodo.11137133).

## Acknowledgments

The authors have no conflicts of interest to report. KY acknowledges support from Future Investigators in NASA Earth and Space Science and Technology (FINESST) Award 80NSSC21K1625. TD acknowledges support from the U.S. National Science Foundation through award 1948955 and from NASA through award 80NSSC22K0155. DAS acknowledges support from the Department of Energy Advanced Research Project Agency (ARPA-E) through award DE-AR0001559 and NASA via award 80NSSC17K0692.

## ORCID iDs

Kana Yamamoto https://orcid.org/0009-0007-3151-9234
Tim DeVries https://orcid.org/0000-0002-7771-9430
David A Siegel https://orcid.org/0000-0003-1674-3055

## References

Arora V K *et al* 2020 Carbon–concentration and carbon–climate feedbacks in CMIP6 models and their comparison to CMIP5 models *Biogeosciences* **17** 4173–222

Bach L T 2024 The additionality problem of ocean alkalinity enhancement *Biogeosciences* **21** 261–77

Bach L T, Gill S J, Rickaby R E M, Gore S and Renforth P 2019 $CO_2$ removal with enhanced weathering and ocean alkalinity enhancement: potential risks and co-benefits for marine pelagic ecosystems *Front. Clim.* **1** 476698

Bach L T, Ho D T, Boyd P W and Tyka M D 2023a Toward a consensus framework to evaluate air–sea $CO_2$ equilibration for marine $CO_2$ removal *Limnol. Oceanogr. Lett.* **8** 685–91

Bach L T, Tamsitt V, Baldry K, McGee J, Laurenceau-Cornec E C, Strzepek R F, Xie Y and Boyd P W 2023b Identifying the most (cost-)efficient regions for $CO_2$ removal with iron fertilization in the southern ocean *Glob. Biogeochem. Cycles* **37** e2023GB007754

Bates N, Astor Y, Church M, Currie K, Dore J, Gonaález-Dávila M, Lorenzoni L, Muller-Karger F, Olafsson J and Santa-Casiano M 2014 A time-series view of changing ocean chemistry due to ocean uptake of anthropogenic $CO_2$ and ocean acidification *Oceanography* **27** 126–41

Boyer T P *et al* 2018 World ocean atlas 2018 *Temperature, Salinity, Phosphate, and Silicate* (NOAA National Centers for Environmental Information. Dataset) (available at:

www.ncei.noaa.gov/archive/accession/NCEI-WOA18) (Accessed 2021)
Broecker W S and Peng T-H 1974 Gas exchange rates between air and sea *Tellus* **26** 21–35
Clarke L, Edmonds J, Jacoby H, Pitcher H, Reilly J and Richels R 2007 Scenarios of greenhouse gas emissions and atmospheric concentrations. sub-report 2.1A of synthesis and assessment product 2.1 by the U.S *Climate Change Science Program and the Subcommittee on Global Change Research Department of Energy* (Office of Biological & Environmental Research) p 154
DeVries T 2014 The oceanic anthropogenic $CO_2$ sink: storage, air-sea fluxes, and transports over the industrial era *Glob. Biogeochem. Cycles* **28** 631–47
DeVries T 2022 Atmospheric $CO_2$ and sea surface temperature variability cannot explain recent decadal variability of the ocean $CO_2$ *sink Geophys. Res. Lett.* **49** e2021GL096018
DeVries T and Primeau F 2011 Dynamically and observationally constrained estimates of water-mass distributions and ages in the global *ocean J. Phys. Oceanogr.* **41** 2381–401
Doney S C, Wolfe W H, McKee D C and Fuhrman J G 2024 The science, engineering, and validation of marine carbon dioxide removal and storage *Annu. Rev. Mar. Sci.* **17**
Eisaman M D, Parajuly K, Tuganov A, Eldershaw C, Chang N and Littau K A 2012 $CO_2$ extraction from seawater using bipolar membrane electrodialysis *Energy Environ. Sci.* **5** 7346–52
Fakhraee M, Li Z, Planavsky N J and Reinhard C T 2023 A biogeochemical model of mineral-based ocean alkalinity enhancement: impacts on the biological pump and ocean carbon uptake *Environ. Res. Lett.* **18** 044047
Fassbender A J, Rodgers K B, Palevsky H I and Sabine C L 2018 Seasonal asymmetry in the evolution of surface ocean $pCO_2$ and pH thermodynamic drivers and the influence on sea-air $CO_2$ flux *Glob. Biogeochem. Cycles* **32** 1476–97
Foteinis S, Campbell J S and Renforth P 2023 Life cycle assessment of coastal enhanced weathering for carbon dioxide removal from air *Environ. Sci. Technol.* **57** 6169–78
Friedlingstein P *et al* 2023 Global carbon budget 2023 *Earth Syst. Sci. Data* **15** 5301–69
Fuss S *et al* 2018 Negative emissions—part 2: costs, potentials and side effects *Environ. Res. Lett.* **13** 063002
Goris N, Tjiputra J F, Olsen A, Schwinger J, Lauvset S K and Jeansson E 2018 Constraining projection-based estimates of the future north atlantic carbon uptake *J. Clim.* **31** 3959–78
Hartmann J, West A J, Renforth P, Köhler P, De La Rocha C L, Wolf-Gladrow D A, Dürr H H and Scheffran J 2013 Enhanced chemical weathering as a geoengineering strategy to reduce atmospheric carbon dioxide, supply nutrients, and mitigate ocean acidification *Rev. Geophys.* **51** 113–49
He J and Tyka M D 2023 Limits and $CO_2$ equilibration of near-coast alkalinity enhancement *Biogeosciences* **20** 27–43
Herzog H, Caldeira K and Reilly J 2003 An issue of permanence: assessing the effectiveness of temporary carbon storage *Clim. Change* **59** 293–310
Ho D T, Bopp L, Palter J B, Long M C, Boyd P W, Neukermans G and Bach L T 2023 Monitoring, reporting, and verification for ocean alkalinity enhancement *State Planet* **2-oae2023** 1–12
Holzer M, DeVries T and de Lavergne C 2021 Diffusion controls the ventilation of a pacific shadow zone above abyssal overturning *Nat. Commun.* **12** 4348
IPCC 2022 Summary for policymakers *Climate Change 2022: Mitigation of Climate Change. Contribution of Working Group III to the Sixth Assessment Report of the Intergovernmental Panel on Climate Change* ed P R Shukla *et al* (Cambridge University Press) 10.1017/9781009157926.001
Jones D C, Ito T, Takano Y and Hsu W-C 2014 Spatial and seasonal variability of the air-sea equilibration timescale of carbon dioxide *Glob. Biogeochem. Cycles* **28** 1163–78
Kanamitsu M, Ebisuzaki W, Woollen J, Yang S-K, Hnilo J J, Fiorino M and Potter G L 2002 NCEP-DOE AMIP-II reanalysis (R-2) *Bull. Am. Meteorol. Soc.* **83** 1631–43
Keith D W, Ha-Duong M and Stolaroff J K 2006 Climate strategy with $CO_2$ capture from the air *Clim. Change* **74** 17–45
Keller D P, Lenton A, Littleton E W, Oschlies A, Scott V and Vaughan N E 2018 The effects of carbon dioxide removal on the carbon cycle *Curr. Clim. Change Rep.* **4** 250–65
Köhler P, Abrams J F, Völker C, Hauck J and Wolf-Gladrow D A 2013 Geoengineering impact of open ocean dissolution of olivine on atmospheric $CO_2$, surface ocean pH and marine biology *Environ. Res. Lett.* **8** 014009
Lauvset S K *et al* 2016 A new global interior ocean mapped climatology: the 1°x1° GLODAP version 2 *Earth Syst. Sci. Data* **8** 325–40
Michaelowa A, Hermwille L, Obergassel W and Butzengeiger S 2019 Additionality revisited: guarding the integrity of market mechanisms under the paris agreement *Clim. Policy* **19** 1211–24
National Academies of Sciences, Engineering, and Medicine 2019 *Negative Emissions Technologies and Reliable Sequestration: A Research Agenda* (National Academies Press) (available at: www.nap.edu/catalog/25259)
National Academies of Sciences, Engineering, and Medicine 2022 *A Research Strategy for Ocean-based Carbon Dioxide Removal and Sequestration* (National Academies Press) (available at: www.nap.edu/catalog/26278)
Nowicki M, DeVries T and Siegel D A 2024 The influence of air-sea $CO_2$ disequilibrium on carbon sequestration by the ocean's biological pump *Glob. Biogeochem. Cycles* **38** e2023GB007880
Oschlies A 2009 Impact of atmospheric and terrestrial $CO_2$ feedbacks on fertilization-induced marine carbon uptake *Biogeosciences* **6** 1603–13
Riahi K, Gruebler A and Nakicenovic N 2007 Scenarios of long-term socio-economic and environmental development under climate stabilization *Technol. Forecast. Soc. Change* **74** 887–935
Riebesell U, Körtzinger A and Oschlies A 2009 Sensitivities of marine carbon fluxes to ocean change *Proc. Natl Acad. Sci.* **106** 20602–9
Siegel D A, DeVries T, Doney S C and Bell T 2021 Assessing the sequestration time scales of some ocean-based carbon dioxide reduction strategies *Environ. Res. Lett.* **16** 104003
van Heuven S, Pierrot D, Rae J W B, Lewis E and Wallace D W R 2011 *MATLAB Program Developed for $CO_2$ System Calculations ORNL/CDIAC-105b Carbon Dioxide Information Analysis Center* (Oak Ridge National Laboratory, U.S. Department of Energy) 10.3334/CDIAC/otg.CO2SYS_MATLAB_v1.1
Wang H, Pilcher D J, Kearney K A, Cross J N, Shugart O M, Eisaman M D and Carter B R 2023 Simulated impact of ocean alkalinity enhancement on atmospheric $CO_2$ removal in the Bering Sea *Earth's Future* **11** e2022EF002816
Wanninkhof R 2014 Relationship between wind speed and gas exchange over the ocean revisited *Limnol. Oceanogr.: Methods* **12** 351–62
Yang A J K and Timmermans M-L 2024 Assessing the effective settling of mineral particles in the ocean with application to ocean-based carbon-dioxide removal *Environ. Res. Lett.* **19** 024035